# TOWARDS AN EFFICIENT ARC SIMULATION FRAMEWORK

R. Fuchs\*, M. Mürmann, H. Nordborg

*Institute for Energy Technology, HSR University of Applied Sciences Rapperswil, Oberseestrasse 10, 8640 Rapperswil, Switzerland*

\* roman.fuchs@hsr.ch

**Abstract.** Arc simulations require a coupled solution of the flow and electromagnetic equations. Despite of industrial interest, there is no established simulation framework available yet. We assess the usability of STAR-CCM+ for low voltage circuit breaker simulations using a test case of a model arc chamber, since this toolkit allows to define and control the simulation in a single environment. In spite of a partially implemented arc root model, the results agree well with reference data of previous publications.

**Keywords:** arc simulation, arc root model, splitter plates, low voltage circuit breakers, computational magnetohydrodynamics.

## 1. Introduction

Electrical arcs occur, for instance, in circuit breakers and other electrical devices that are required for safe operation of a power grid network and its components connected to. Arcs may be created by separating two electrodes while current is flowing (for a detailed description see, e.g., [1]). Hence, a thermal plasma is formed which shows as an intensive source of light and energy at elevated temperature levels. Therefore, circuit breakers must be designed appropriately to withstand the thermal loads and forces due to an explosive gas expansion. The basic principle for arc quenching is to raise its voltage above the grid voltage, which is achieved by arc elongation and efficient cooling of the plasma. Additionally, in low voltage circuit breakers, the preferred method is to drive the arc into a quenching chamber with several ferromagnetic splitter plates. Therein, the arc is split into multiple branches, and because each arc root leads to an additional voltage drop, it becomes extinguished.

Experiments are essential in circuit breaker development, but the short timescales and physical conditions make it difficult to measure relevant quantities in sufficient detail and quality. Therefore, numerical simulations of electrical arcs are an important source of information for industrial manufacturers to optimize their products in size, costs, and extension of operational ranges towards higher currents.

A useful simulation framework must cover the relevant physics including electromagnetism, gas dynamics, thermal radiation, material data at elevated temperature levels, evaporation of materials that are in contact or nearby the arc, as well as their mutually coupled effects. For instance, the electrical conductivity of the plasma is a key material parameter, which depends on the gas temperature, pressure, gas composition, and contamination with metal vapor, and couples the Maxwell and Navier-Stokes equations. Additionally, electrode motion must be included and the framework must allow for mesh deformation, remeshing, and data interpolation in a robust manner.

Moreover, the simulation framework must build on appropriate numerical methods. On the one hand, the gas flow solver should rely on the finite volume method to capture accurately the nonlinear effects of shock waves. On the other hand, the electromagnetic equations are to be solved with edge-based finite elements (FE) if ferromagnetic splitter plates are considered. Consequently, an arc simulation framework consists of two or more separate solvers and, frequently, an additional software level that is responsible for synchronization of the solvers and their data exchange. For example, this methodology is used by [2] and works sufficiently well. However, it requires skilled users in multiple programming languages and touching of low-level operations for implementing advanced physical models. A notable amount of time may be spent on programming and debugging rather than the physical modeling of the circuit breaker.

Our research group started using STAR-CCM+ for arc simulations because of its integrated architecture. This framework consists, among others, of a standard set of flow solvers and a recently added FE magnetic vector potential solver. Surface fluxes and volume sources can be defined via field functions on the GUI level with a comprehensive set of operators and building blocks, and without referencing individual mesh cells. The graphical user interface also allows to define and control moving geometries as well as the required remeshing and data interpolation.[3] Data exchange among the solvers is also included automatically and does not require additional software levels. In total, we expect it to be user-friendly and a promising framework for arc simulations.

The capabilities of STAR-CCM+ are currently being assessed by implementation of previously reported arc simulations. Here, we consider a test case based on the works of T. Rüther [4], A. Mutzke [5], and

J. Rüther [6] who investigated a simplified arc chamber with a single splitter plate. They showed that a nonlinear current-voltage characteristic allows to model the arc splitting process accurately compared to experimental observations.

In this paper, we present results on the selected test case of a simplified arc chamber using STAR-CCM+ as a toolkit for arc simulations. Firstly, we define the model geometry and simulation settings. In the main part, we compare our results to those of [6] and we report on the usability of the software framework. Finally, conclusions are drawn.

## 2. Simulation model

### 2.1. Geometry and Mesh

We consider a model arc chamber identical to [6], see figure 1. The parallel arc rails are $1.5 \times 58 \times 4$ mm with 8 mm inner distance, and a splitter plate $1 \times 20 \times 4$ mm located centrally between them. The plasma is computed in a box that starts 16 mm above the lower electrode ends, with an outlet at the upper boundary. The arc is ignited 7 mm below the splitter plate with a radius of 1 mm. An auxiliary cylinder with elliptic cross section (15 and 10 mm semiaxis) contains the plasma and electrode domains so that the magnetic boundary conditions can be specified in the farfield.

The domain is discretized with a polyhedral mesh for all solvers. The cell size is 0.25 mm in the plasma domain, with increasing element size in the elliptic cylinder. Prism layers are specified in the plasma domain with a total thickness of 0.1 mm.

### 2.2. Governing equations

The compressible Navier-Stokes equations for laminar flow are solved including source terms for the Lorentz force and Ohmic heating. Radiation is included by the discrete ordinate method with mean absorption coefficients given in 6 bands. Absorption coefficients of air and band boundaries are identical to [6].

The electromagnetic equations are solved in the low-frequency and magnetostatic limit. The magnetic vector potential is computed with an iterative solver in finite volumes, because all material data have a relative permeability $\mu_r = 1$. The voltage drop in the arc roots is modeled according to [5], and is specified at the contact interface between the electrodes and the air domain. The characteristic current-voltage curve consists of two exponential functions such that the curve has a peak voltage drop of 19.7 V at a current density of 13 kA m$^{-2}$ and a constant voltage drop of 10 V for large current densities.

In contrast to [6], the energy equation is solved only in the plasma domain with adiabatic boundary conditions. The Ohmic heating due to the voltage drop at the interfaces is neglected. A more complete arc root model is not in the focus of this study and is left to subsequent work that will also include source terms for the mass, momentum, and energy equations due to metal evaporation.
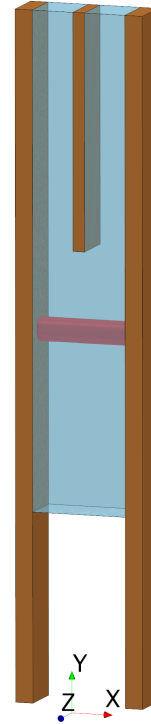


*Figure 1. Model arc chamber geometry with the copper parts, the air volume, and the arc column at its initial position.*

### 2.3. Material data

Material data for the copper electrodes and air are provided by STAR-CCM+ using the Equilibrium Air model [7]. The electric conductivity for air is tabulated according to [8], and limited to a minimum value of $\sigma = 10^{-3}$ S m$^{-1}$ due to numerical reasons.

### 2.4. Boundary and initial conditions

A pressure outlet condition is specified at the surfaces located at y = 58 mm; otherwise, wall boundary conditions are used for the gas flow. The gas is initially at rest and at ambient temperature (T = 300 K).

Electric boundary conditions are applied to the lower ends of the parallel rails. The right electrode is at zero potential, while the left electrode is stressed with a sinusoidal total current corresponding to a peak value of 1 kA effective at 50 Hz. A time-delay of 500 µs is included which is in accord with the ignition time in the experiments by [4]; the initial total current is therefore equal to 221 A.

The ignition wire is modeled as an electrically conductive channel with 1 mm radius and conductivity $\sigma = 10^4$ S m$^{-1}$ until $t = 15$ µs.

The simulation time step is 0.5 µs uniformly with 40 inner iterations per time step. In the first time step, the solvers are iterated for 100 inner steps to ensure a converged solution. The radiative heat flux is computed only in the first inner iteration per time step to save computing time.
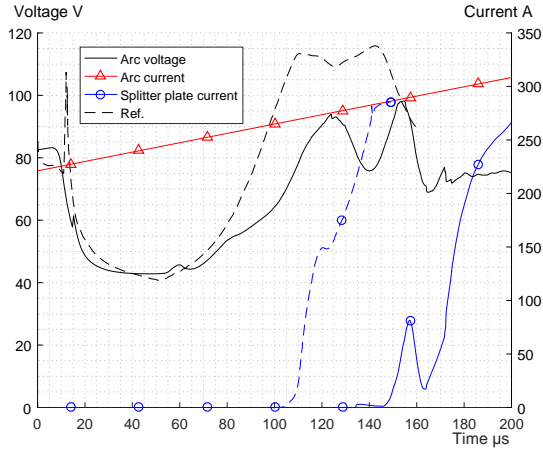
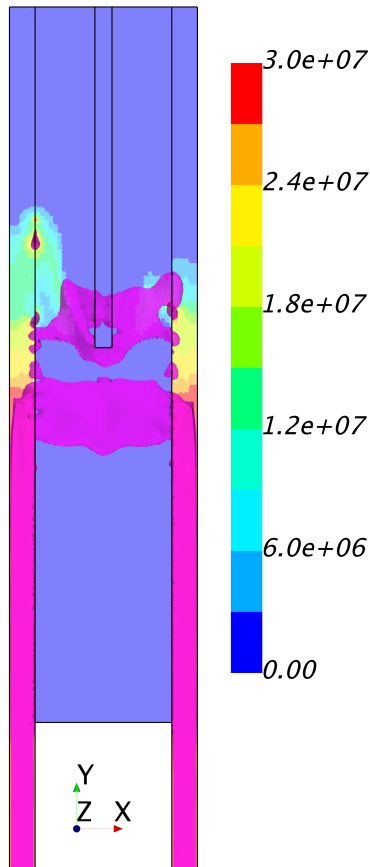*Figure 2. Graphs of arc voltage and currents in comparison to the reference data (figure 3-5 in [6]).*



*Figure 3. Electric current density at $t = 155\,\mu s$ on central section plane. The isocontour value is at $3 \times 10^7\,A\,m^{-2}$ and shown in magenta.*

## 3. Results and Discussion

Figure 2 shows the arc voltage, total arc current, and the current through the splitter plate as a function of time from ignition until $t = 200\,\mu s$. Also shown are the reference data from figure 3–5 in [6] which is given until $t = 160\,\mu s$. The total arc current is given as a boundary condition and increases from 221 A to 310 A.

Initially, the arc voltage is 83 V and decreases after $t = 6\,\mu s$ towards a minimum value of 43 V at $t = 46\,\mu s$. The jump at $t = 15\,\mu s$ is due to the minimum condition for the plasma electrical conductivity modeling the arc ignition phase. After $t = 55\,\mu s$, the arc voltage increases and shows two maxima of 90 V at $t = 125$ and 95 V at 155 $\mu s$, before it tends to a rather constant value of 75 V. The splitter plate current is zero until $t = 135\,\mu s$, when a small current is noted. Then, the current reaches a maximum of 81 A at $t = 155\,\mu s$. After reducing to 18 A in 10 $\mu s$, it raises towards the total current. Figure 3 illustrates the situation at the splitter current peak at $t = 155\,\mu s$. We see that a partial current flows through the splitter plate while the major part of the current flows through the plasma below. We also see distinguished arc roots on both rails.

The data is explained as follows with reference to graphical visualizations. Until $t = 55\,\mu s$, the arc remains stationary and heats the nearby plasma resulting in a low arc voltage. Then, the pressure wave reflected from the lower boundary pushes the arc upwards into a cooler domain and results in increasing voltage due to elongated arc length and lower temperature. At $t = 60\,\mu s$, new arc roots are formed symmetrically on the rails reducing the arc voltage slightly. At $t = 80\,\mu s$, the arc reaches the splitter plate. Another pair of arc roots are formed above the lower end of the splitter plate while those at the initial position vanish. Hence, the arc column becomes M-shaped enclosing the splitter plate and while the arc becomes elongated, the arc voltage increases more steeply. Subsequently, the arc stays near the edge of the splitter plate and starts to burn more diffusely below it without being split and moving onto the splitter plate. This is in contrast to [6] and is due to insufficient voltage difference between the arc loop along the interface and the required voltage for arc root formation as modeled by the characteristic current-voltage curve. Additional attempts are required to overcome the arc root formation voltage on the splitter current, explaining the two voltage and current maxima between $t = 120\,\mu s$ and $t = 170\,\mu s$.

Comparison to the reference data shows that our arc voltage is comparable until $t = 70\,\mu s$. Subsequently, different arc splitting behavior is observed which is attributed to the incompletely implemented arc root model and different material data. Other differences exist in the radiation model: here, the discrete ordinate model is used whereas in [6] a combination of net emission coefficients and increased heat conduction due to radiation have been used. Despite these differences, the arc voltage and the timescale for arc splitting are comparable.

The main objective of this study is to evaluate the simulation framework provided by STAR-CCM+ for arc simulations. The results presented above show that it is a viable toolkit. The user-friendly and modern graphical user interface supports the user in setting

up the simulation and implementing advanced arc root models. We take it as an advantage that the simulation may be controlled in a single window. Material data can be loaded as multivariate file tables without writing and loading additional user code. Moreover, the user can focus more on plasma modeling rather than programming tasks.

## 4. Conclusions

We used a model arc chamber referring to a low voltage circuit breaker as a test case to evaluate STAR-CCM+ as a possible step forward to more efficient arc simulations in industry and research. We implemented a macroscopic model for the voltage drop at the electrode- plasma interface as a current-voltage characteristic that is applied at the corresponding geometric interfaces. Further source terms of a complete arc root model will be implemented similarly in future work. Despite the partially implemented model, the results showed that this model allows to capture the main aspects of arc splitting in a quenching chamber. In comparison to [6], differences are attributed to model settings and material data. The simulations ran robustly and are easily handled because the solvers are coupled and managed in a single graphical user interface.

In total, we are satisfied with the capabilities of STAR-CCM+ for arc simulations, and we will continue assessing it in further applications of high- and low-voltage plasma simulations.

### Acknowledgements

### References

[1] Eduard Vinaricky, editor. *Elektrische Kontakte, Werkstoffe und Anwendungen: Grundlagen, Technologien, Prüfverfahren.* Springer Berlin Heidelberg, Berlin and Heidelberg, 3. edition, 2016.

[2] Christian Rümpler. *Lichtbogensimulation für Niederspannungsschaltgeräte.* Fraunhofer-Verl., Stuttgart, 2009.

[3] Roman Fuchs, Mario Mürmann, Henrik Nordborg, and Paul Hilscher. Electric arc simulations - towards a user-friendly and efficient tool for industry. In *Nafems World Congress*, 2017.

[4] Thomas Rüther. *Experimentelle Untersuchung der Lichtbogenaufteilung an Löschblechen.* Cuvillier, Göttingen, 2008.

[5] Alexandra Miriam Mutzke. *Lichtbogen-Simulation unter besonderer Berücksichtigung der Fusspunkte.* Ingenieurwissenschaften. Verl. Dr. Hut, München, 2009.

[6] Julia Rüther. *Weiterentwicklung und Vereinfachung eines Simulationsmodells für Schaltlichtbögen in Löschblechkammern.* Energietechnik. Verl. Dr. Hut, München, 2014.

[7] R. N. Gupta, K.-P. Lee, R. A. Thompson, and J. M. Yos. Calculations and curve fits of thermodynamic and transport properties for equilibrium air to 30000 K. *NASA STI/Recon Technical Report N*, 92, 1991.

[8] A. D'Angola, G. Colonna, C. Gorse, and M. Capitelli. Thermodynamic and transport properties in equilibrium air plasmas in a wide pressure and temperature range. *The European Physical Journal D*, 46(1):129–150, 2008. `doi:10.1140/epjd/e2007-00305-4`.